NANOSYSTEMS:
PHYSICS, CHEMISTRY, MATHEMATICS

Showket S., et al. *Nanosystems: Phys. Chem. Math.*, 2024, **15** (3), 418–428.
http://nanojournal.ifmo.ru
DOI 10.17586/2220-8054-2024-15-3-418-428

Original article

Investigation of sensing performance of silicene nanoribbon towards methanol and ethanol molecules: A computational study

Shazia Showket[1], Khurshed A. Shah[2], Ghulam N. Dar[1], Muzaffar Ali Andrabi[3]

[1]Department of Physics, University of Kashmir, Srinagar, J&K–190006, India

[2]Postgraduate Department of Physics, Sri Pratap College, Cluster University Srinagar, J&K–190001, India

[3]Department of Applied Sciences, Institute of Technology, University of Kashmir, Srinagar, J&K–190006, India

Corresponding author: Dr. Khurshed A. Shah, drkhursheda@gmail.com

ABSTRACT In this work, we perform an intricate computational analysis to investigate the adsorption mechanism of human breath exhaled VOCs, namely, methanol and ethanol, along with interfering water vapour on the surface of armchair silicene nanoribbon (ASiNR) by employing density functional theory to analyse the structural, electronic, and transport properties. The findings indicate that the most favorable adsorption configuration for methanol and ethanol involves the hydroxyl group (-OH) oriented towards the silicene surface, after optimisation. Moreover, we have calculated the adsorption energies which shows that ethanol is strongly physisorbed than methanol and water molecules on the ASiNR surface. Apart from that, the results of IV characteristics, transmission spectra and density of states corroborate these observations. In addition, we have computed the sensitivity (%), the results of which revealed that methanol demonstrates a high sensitivity of 42 % compared to other molecules towards the surface of ASiNR. Furthermore, the recovery time of the sensor was found to be extremely long, which indicates that ASiNR based device has great potential for use as disposable sensors and scavengers for toxic gas molecules.

KEYWORDS armchair silicene nanoribbon, DFT, volatile organic compounds, sensitivity

ACKNOWLEDGEMENTS This work has been supported by JKST&IC funded project (Grant No. JKST&IC/SRE/1172-74) and SERB (Grant No. CRG2022/006428-G).

FOR CITATION Showket S., Shah K.A., Dar G.N., Ali Andrabi M. Investigation of sensing performance of silicene nanoribbon towards methanol and ethanol molecules: A computational study. *Nanosystems: Phys. Chem. Math.*, 2024, **15** (3), 418–428.

1. Introduction

The swift advancement of industrial technology and contemporary living have made gas detectors indispensable for safeguarding both the environment and human health [1, 2]. The diagnosis of diseases and the biological field are two important uses for gas sensors. Among many diseases, malignancies have been identified as one of the largest and most significant categories. Prostate and lung cancers are among the most common types of tumours that cause death in this group. Gas sensors, being a noninvasive technology, have the potential to aid in the early diagnosis of cancer by identifying cancer biomarkers in patients' exhaled breath [1, 3, 4]. A great deal of work has gone into finding cancer biomarkers, and it has been found that distinct volatile organic compound (VOC) patterns are associated with various diseases and cancers [5–7]. Breath, as everyone knows, contains about a thousand different types of volatile organic compounds (VOCs) at quantities ranging from parts per million to parts per trillion (ppmv to pptv) [8,9]. Common volatile organic compounds (VOCs) found in human breath include alcohols, ketones, and toluene. These can be measured and identified using a variety of methods, but one interesting method is the use of gas sensors based on nanomaterials [10]. It is important to note, though, that fuel combustion, industry, and transportation all produce exhaust fumes, which are another source of VOCs [11]. Thus, the detection of these gas molecules appears to be essential for environmental safety and monitoring.

Since the revelation of graphene, 2D materials, characterized by their substantial surface area-to-volume ratio, have garnered significant attention from scientists as potential options. Notable examples include silicene, germanene, stanene, and transition-metal dichalcogenides, owing to their remarkable electrical, magnetic, optical, and gas sensing capabilities [12–15]. Silicene, an allotrope of silicon with a two-dimensional hexagonal lattice structure akin to graphene, is a focal point of research due to its exceptional properties and potential applications in the field of nanoelectronics [16–19]. Silicene lacks a band gap, however, due to its unique buckled structure, its band gap can be easily adjusted using various techniques [20–26]. Despite the fact that free standing silicene is not stable, it was experimentally fabricated on Ag [27], Ir [28], ZrB_2 [29] and ZrC [30]. The extraordinary properties of silicene including ferromagnetism [31], half metallicity [32], quantum Hall effect [33], giant magnetoresistance [34], and superconductivity [35] along with its compatibility with silicon based nanoelectronics may give edge to silicene rather than graphene. Though silicene is a zero-band gap

material, the band gap issue can be resolved by slicing it into strips called silicene nanoribbons (SiNRs). Substrates like; Ag (100), Ag (110), Au (110) [36–39] have been used to generate SiNRs. An array of highly uniform parallel SiNRs having width of $\sim$ 1.7 nm have been synthesised by Afuray et al. on Ag (110) substrate [36]. When it comes to gas nanosensor applications, nanoribbons are more appealing than sheets because of their intrinsic band gap, small dimensions, and free reactive edges. Armchair silicene nanoribbons (ASiNRs) and zigzag silicene nanoribbons (ZSiNRs) are the two types of SiNRs [40]. ASiNRs have been chosen because adsorption of gases has comparatively smaller effect on electronic properties of ZSiNRs [41].

Numerous researches [42–44] suggest that silicene holds a great promise for gas sensing applications. However, the majority of these studies primarily focused on basic gases such as; CO, NO, NO_2, NH_3 and CH_4, CO_2. Moreover, silicene [45–47] and other 2D materials [9,48] have also been explored for the sensing applications of VOCs. These findings highlight silicene's potential as a highly effective sensor, inspiring us to further develop it for the detection of harmful VOCs, including methanol and ethanol. To investigate the viability of employing silicene for the development of volatile organic compound (VOC) sensors, we performed rigorous calculations utilizing density functional theory. This analysis encompasses a comprehensive examination of various facets, including electronic properties (such as adsorption energy, interaction distance, and density of states), structural attributes (bond length and buckling distance), transport characteristics (transmission spectra and conductance), as well as sensitivity (%) and recovery time (τ). The aim is to elucidate and quantify the intricate interplay between the surface of ASiNR and VOCs, providing valuable insights into the material's potential as a highly efficient sensor for volatile organic compounds. Numerous investigations have been conducted by the researchers to examine the adsorption characteristics of Volatile Organic Compounds (VOCs), encompassing methanol and ethanol, on diverse substrates. These substrates include Pd-decorated Phosphorene [49], Al-doped GeS [50] and green phosphorene nanosheets [51]. Moreover, the study has highlighted the efficacy of graphyne nanosheets as a sensing material for methanol and ethanol, indicating a preferential adsorption of ethanol over methanol [52], Additionally, $MoSe_2$ monolayers have been identified as effective chemi-resistors for the detection of methanol and ethanol vapors in the ambient environment, as elucidated in the research paper authored by V. Nagarajan et al. [53].

In the current study, our central objective is dedicated to scrutinizing the structural, electronic, and transport characteristics of armchair silicene nanoribbon (ASiNR) for the purpose of sensing VOCs (methanol and ethanol) and water molecule. Our empirical observations indicate that the simulated armchair silicene nanoribbon-based two-probe device holds considerable promise as disposable sensor and scavenger for toxic gas molecules within the ambient environment.

2. Models and methods

In the ongoing study, we have modelled a 7 atom-wide armchair silicene nanoribbon (ASiNR) comprising 108 atoms. To assess the structural, electronic, and transport characteristics, we have configured it as a two-probe device, delineated into three distinct regions: the left electrode, the central scattering region, and the right electrode. The lattice constant of the optimized silicene is determined to be 3.85 angstroms (Å) [54]. The parameters for the silicon-silicon bond length and buckling height were selected as 2.28 and 0.44 Å, respectively, in adherence to the established standard values [24]. The length of two electrodes was considered to be 6.72Å. The integration of the ASiNR system with electrodes was undertaken to vanquish the current quantization effects induced by contact regions. To assess the potential adsorption of volatile organic compounds (VOCs) on the surface of the ASiNR model, a thorough analysis was conducted through Density Functional Theory (DFT) based first principles computations utilizing the Quantum Atomistix Toolkit (ATK) software [55]. Current calculations have been executed utilizing the Landauer–Buttiker formula [56], conjoined with Non-Equilibrium Greens Function (NEGF) formalism, as articulated by the following expression:

$$I = \frac{2e}{h} \int_{-\infty}^{\infty} T\left(E, V_b\right) \left[f\left(E - \mu_L\right) - f\left(E - \mu_R\right)\right] dE, \tag{1}$$

where $T\left(E, V_b\right)$ represents the transmission function at a given energy E and voltage V_b, while, $(E - \mu_L)$ and $(E - \mu_R)$ denote the Fermi distribution functions of the left and right electrodes, respectively.

To evaluate the alterations in various sensing properties including the adsorption energy, interaction distance, IV curves, transmission spectra, projected device density of states (PDDOS), sensitivity (%), selectivity and recovery time (τ), both alcohol molecules were positioned proximate to the ASiNR surface. The models were simulated using density functional theory with an electrode temperature of 300 K and the density mesh cut-off was set at 75 Hartree. The maximum range for the interaction was taken as 10 Å and the Fourier 2D solver was approved as the poisson solver for the boundary conditions. The potential difference applied between the two electrodes ranged from 0 to 2 volts to scrutinize the current flowing across the models. Additionally, the exchange-correlation functional of Perdew, Burke, and Ernzerhof (PBE) type [57] coupled with the Double Zeta Polarized (DZP) basis set [58] has been employed to facilitate the relaxation of the geometrical structures of the ASiNR models adsorbed with two alcohol molecules, namely, methanol and ethanol. A vacuum space of 15 Å was taken into consideration, in the x and y directions where the structures lack periodicity, to abstain the mirrored interactions. In the pursuit geometry optimization, the Brillouin zone has been thoroughly sampled using a grid resolution of $1 \times 1 \times 21$ k-points [59, 60] and for calculating the total energy, and electron

transport properties, Monkhorst–Pack Scheme is used with a k-point grid of $1 \times 1 \times 100$ (z-direction along the ASiNR increasing direction) [59–62]. Preceding the computational analyses, exhaustive optimization procedures were applied to all structures, ensuring that both force tolerance and the corresponding lattice stress reached values below 0.05 eV/Å and 0.0005 eV/Å^3 respectively with the maximum step size of 0.2 Å. The optimization process was executed by employing the limited memory Broyden–Fletcher–Goldfarb–Shanno (LBFGS) algorithm.

3. Results and discussion

Since ASiNRs having width $L = 3n$ or $L = 3n + 1$ (where n is an integer) are known to express semiconducting behaviour [63], we construct an ASiNR with a width of 7 atoms. To ensure the stability of the edges, the dangling bonds of the silicon atoms at the edges of the ASiNR are passivated on both sides with hydrogen atoms. Because of the incomplete sp^3 hybridization in silicene and the heightened reactivity of the edges compared to the surface, the surface is left unaltered [64–66]. As per reports, the paramagnetic semiconductor 7-ASiNR exhibits a band gap of 0.54 eV [62, 67]. The semiconducting ASiNR was selected based on the presumption that the adsorption of gas molecules has a significantly diminished impact on the electrical characteristics of metallic zigzag SiNRs (ZSiNRs). We design the ASiNR into a two-probe device with three regions: the left electrode, the central scattering region, and the right electrode for calculating the sensing properties. The design structure of our proposed ASiNR device is shown in Fig. 1, where, the bond lengths between Si–Si and Si–H, are outlined as 2.28 and 1.43 Å, respectively, across the three regions.

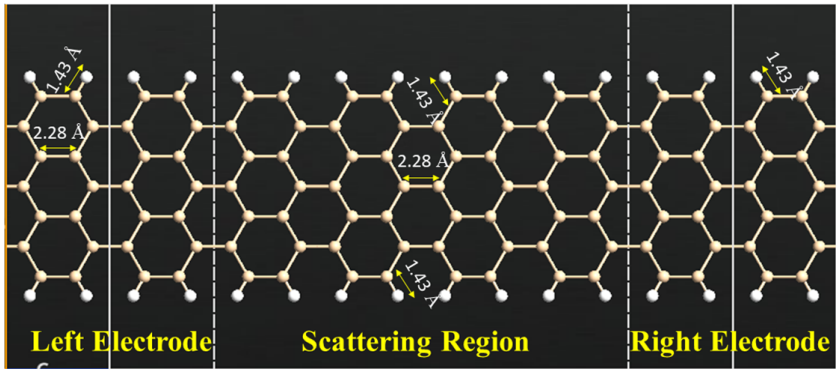

FIG. 1. The modeled ASiNR device comprising of the left electrode, the central scattering region & the right electrode. The upper and lower white balls represent the passivated H-atoms

3.1. Sensing profile

3.1.1. Structural configuration. After optimising the ASiNR models, it was found that the adsorption process induces a subtle deformation in both the base and target materials. The bond lengths and buckling heights of the ASiNR modelled devices were calculated before and after adsorption. It was determined that these values exhibited variation in the scattering region ranging from 2.28 to 2.30 Å and 0.44 to 0.60 Å, respectively, for methanol and from 2.28 to 2.29 Å and 0.44 to 0.54 Å, respectively, for ethanol. Additionally, the Si–H bond lengths were also found to vary in the scattering region ranging from 1.43 to 1.50 Å. Moreover, we have also calculated the bond lengths of methanol, ethanol and water molecules, which demonstrate minimal deviation, with the exception being observed in the bond lengths between C–O and O–H, which increase from their standard values after adsorption on the ASiNR models. Specifically, in the case of methanol, the C–O and O–H bond lengths show a variation within the range of 1.39 to 1.45 Å and 0.95 to 0.98 Å, respectively, while, for ethanol, the C–O and O–H bond lengths demonstrate a variation within the range of 1.41 to 1.47 Å and 0.95 to 0.98 Å, respectively. The optimised structures of VOC based sensors are illustrated in Fig. 2, elucidating the most advantageous places of methanol and ethanol on the ASiNR surface after optimisation.

3.1.2. Adsorption response of the target molecules on silicene. To investigate the interactions between the target molecules and ASiNR, we put them 3.5 Å from the ASiNR surface. After complete relaxation, the adsorption behaviour of molecules on the ASiNR device are analysed. It was found that the structural and electronic characteristics of the base-target materials appear to change after optimization. The adsorption energies and interaction distances of both modelled devices were determined in order to figure out the most stable configuration. Our simulated models revealed negative adsorption energy, signifying a substantial reduction in electron cloud repulsion compared to electrostatic contact between the three molecule and the ASiNR. This phenomenon resulted in the adsorption of proposed molecules on the ASiNR surface. The larger the negative value of adsorption energy is, the stronger the contact and consequently the greater is the charge transfer. The adsorption energy (E_{ad}) is computed using the following equation [67, 68]:

$$E_{\text{ad}} = E_{\text{ASiNR+Molecule}} - E_{\text{ASiNR}} - E_{\text{Molecule}}. \tag{2}$$

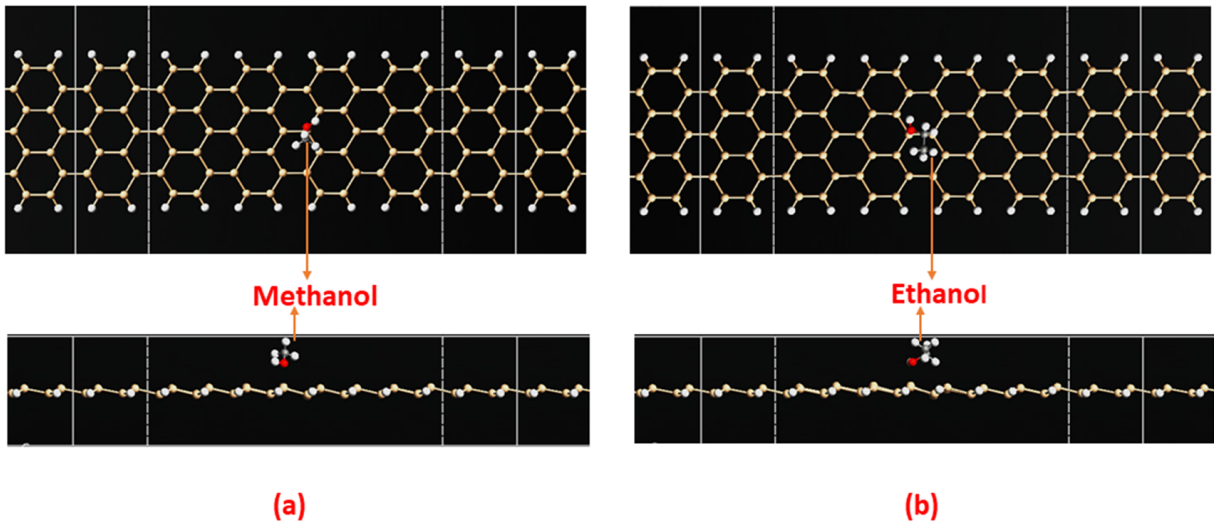

FIG. 2. Top and side views of optimised models of ASiNR with (a) methanol and (b) ethanol

The terms $E_{\text{ASiNR+Molecule}}$, E_{ASiNR}, and E_{Molecule} represent the total energies of the ASiNR-molecule system, pristine ASiNR, and the individual gas molecule, respectively. The interaction distance of 2.20 Å was found for ML and EL, while 2.9 Å in case of water molecule, confirming the Van der Waals type of interaction. It is noteworthy that chemical bonds do not exist in their fully relaxed structures based on the obtained interaction distances. The interaction distance reflects the binding strength, which is inversely proportional to distance [69]. In our computational work, methanol and ethanol were positioned at various places on the surface of ASiNR. The hydroxyl group (-OH) facing the surface of ASiNR models was shown to be the most suitable adsorption configuration of the molecules after optimisation. To have a clear understanding of our observations, we have shown the zoomed side views of the ASiNR modelled devices adsorbed with ML and EL in Fig. 3.

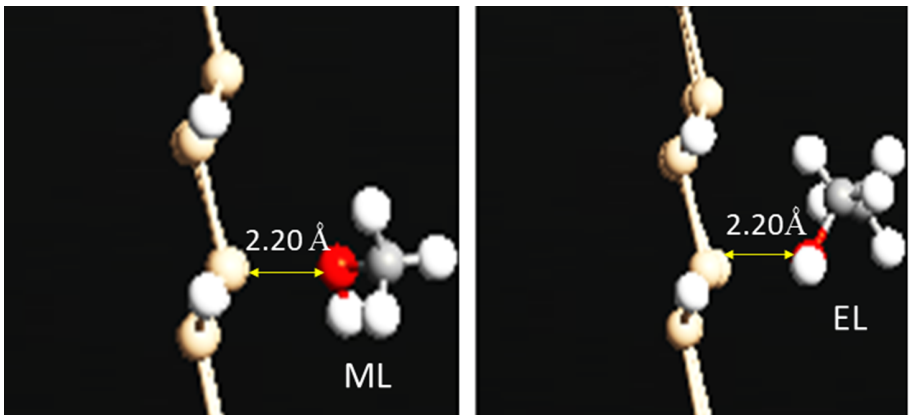

FIG. 3. Zoomed sideview representation of the ASiNR modelled devices with ML and EL at a distance of 2.20 Å respectively after optimisation

Furthermore, the obtained adsorption energy values of -1.56 eV for ML, -1.62 eV for EL and -1.43 eV for water molecule are higher as compared to the previously reported sensors [41–43]. The more negative value of adsorption energy for ethanol suggests a stronger adsorption, leading to a longer recovery time for ASiNR compared to methanol and water molecule (which will be discussed in section 3.1.6).

3.1.3. Transport characteristics:

3.1.3.1. IV Curve. In assessing the sensing capabilities of the ASiNR based device for the proposed gas molecules, a thorough evaluation of the current versus bias voltage was performed by employing a bias voltage range of 0 – 2 V. The findings, as depicted in Fig. 4, distinctly reveal that the threshold voltage for both pristine, and VOC adsorbed ASiNR is 0.63 V. It is noteworthy to note that methanol, ethanol and water molecules are characterized as polar molecules. Consequently, the adsorption process facilitates a direct charge transfer mechanism between the sensor surface and the proposed molecules. This intermolecular interaction leads to an augmentation in the concentration of majority charge carriers, thereby resulting in a discernible elevation in the overall current traversing through the device. This observation underscores the efficacy of the proposed device in detecting and responding to gas molecules through direct charge transfer mechanisms during the adsorption process. Apart from that, an elevation in current observed beyond the threshold bias voltage is a direct consequence of an augmented number of conduction states in close proximity to the Fermi level. In the case of ASiNR adsorbed with methanol, the current registers lower values in comparison to pristine and ASiNR adsorbed with ethanol and water molecules. This disparity can be attributed to lattice distortion, which in turn diminishes the mobility of the sensing device. Additionally, notable peak currents of 38.6, 22.3, 34.8 and 33.7 μA are discerned for pristine, ML-adsorbed, EL-adsorbed and water molecule-adsorbed ASiNR respectively. The low peak currents of ASiNR based sensors compared to pristine one could indeed be attributed to electron withdrawing effects of methanol, ethanol and water molecules. Their adsorption leads to a decrease in the availability of conducting electrons and thus, resulting in lower peak currents. Furthermore, our observations align with existing literature, providing a contextual framework for understanding the implications of these findings. [47, 62, 68].

3.1.3.2. Transmission Spectra. We have carried out a thorough analysis of the electronic transport characteristics, specifically focusing on the transmission spectrum, pertaining to the ASiNR model in the absence and in the presence of two alcohol molecules. Fig. 5 presents a comparative analysis of the transmission spectra, illustrating the distinctions between pristine ASiNR without any adsorption and ASiNR adsorbed with ML and EL.
The comparison was conducted across various bias voltages, specifically at 1.2, 1.8, and 2 V, revealing distinctive electronic transport properties under these conditions. Our observations indicate a remarkable similarity in the transmission spectra of ASiNR models both before and after adsorption, with the notable distinction lying in the values of transmission peaks. As depicted in Fig. 5, it is evident that the transmission probability is at its maximum for ASiNR adsorbed with EL at a bias voltage of 1.2 V. Moreover, the transmission probability is at its minimum for ASiNR adsorbed with ML at a bias voltage of 1.8 V. Furthermore, under a bias voltage of 2 V, the pristine ASiNR, without any adsorption, exhibits the maximum transmission probability. The obtained results are consistent with the previously acquired IV characteristics. Therefore, the fluctuations observed in the transmission spectrum further confirm the device's responsiveness towards the specified alcohol molecules.

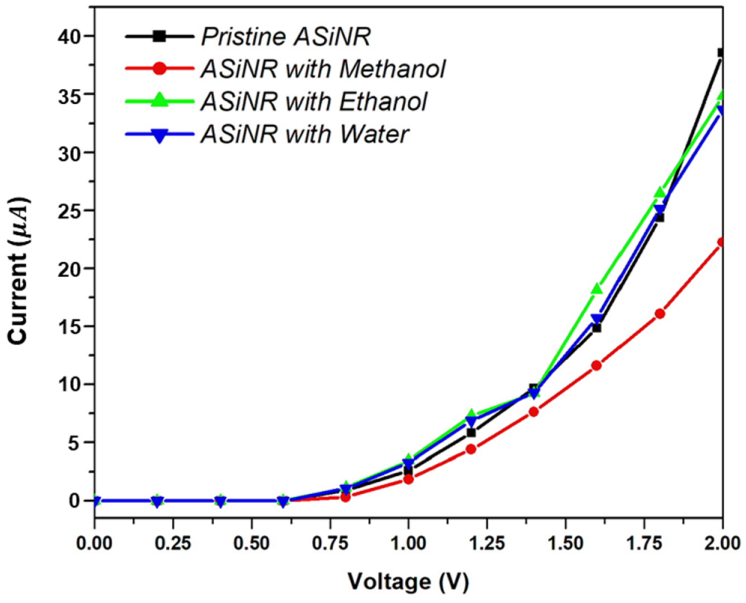

FIG. 4. IV characteristics of Pristine ASiNR and ASiNR adsorbed with methanol, ethanol and water molecules

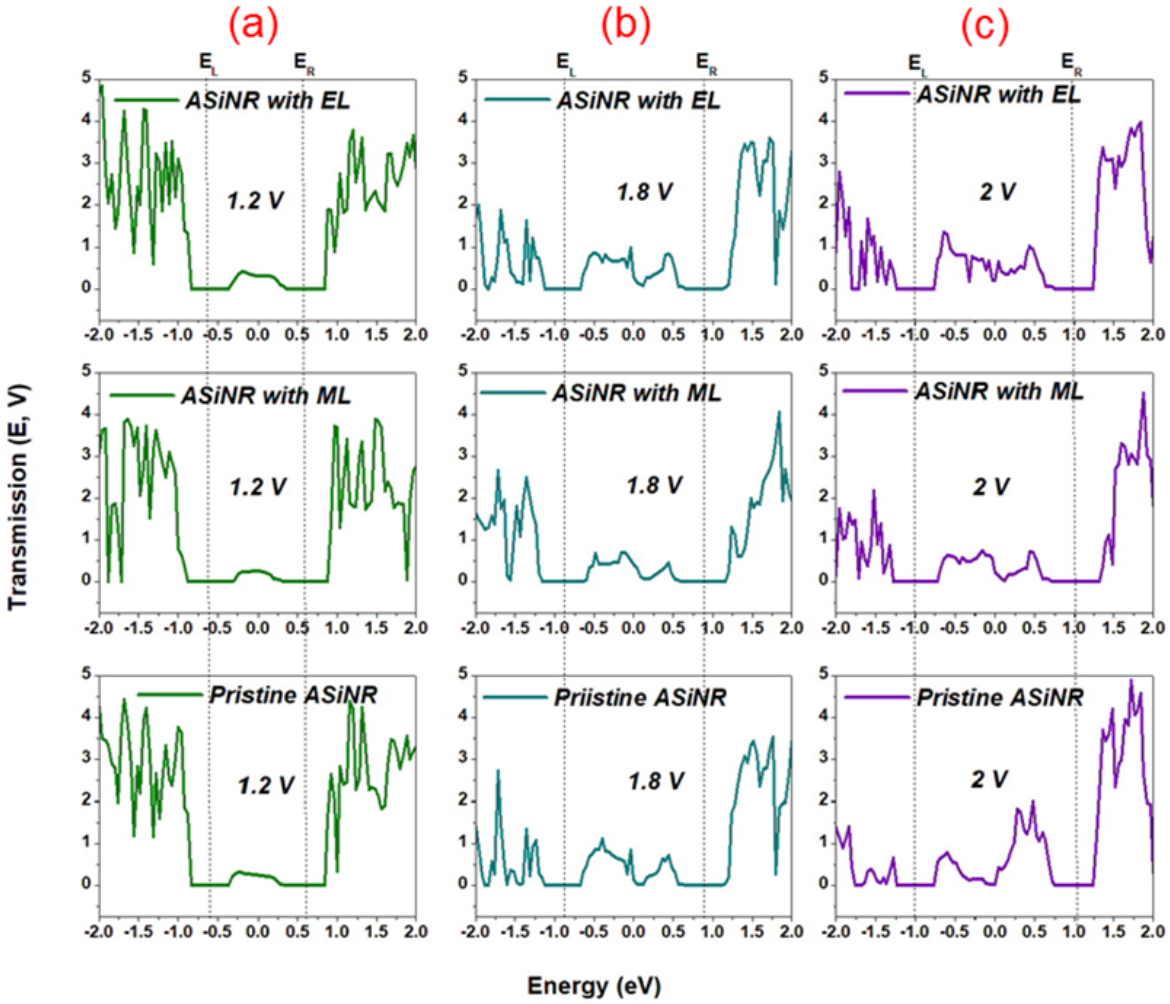

FIG. 5. Transmission Spectra of Pristine ASiNR and ASiNR with ML and EL at (a) 1.2 V, (b) 1.8 V and (c) 2 V

3.1.4. Density of states. The projected device density of states represents the contribution of each atomic orbital to the overall density of states at a specific energy level. In order to comprehend the impact of Volatile Organic Compounds (VOCs) on the electronic characteristics of ASiNR, we have computed the projected device density of states both before and after adsorption. From Fig. 6, it is evident that there are no peaks present around the Fermi level. This observation suggests that ASiNR maintains its semiconducting properties both before and after the adsorption of target molecules. The absence of peaks around the Fermi level additionally supports the conclusion that molecules undergo physisorption on the ASiNR surface. Moreover, these findings align with the adsorption energy and transport characteristics of the modelled device.

3.1.5. Sensitivity (%). To ensure a clear comprehension of the sensing capabilities of ASiNR, we calculated the sensitivity, which is defined as the change in conductance. Initially, we assessed the conductance (I/V) of the ASiNR modelled devices. The calculated conductance was then employed to conduct a focussed analysis on sensitivity, by utilizing the following equation [24].

$$S = \left| \frac{G_{\text{ASiNR+Molecule}} - G_{\text{ASiNR}}}{G_{\text{ASiNR}}} \right|. \tag{3}$$

The terms $G_{\text{ASiNR+Molecule}}$ and G_{ASiNR} represent the conductance of the ASiNR-molecule system and pristine ASiNR respectively. Table 1 lists the sensitivity (%) of the sensor towards the three proposed molecules at 1.2, 1.4, 1.6, 1.8 and 2.0 V.

Notably, at 1.8 and 2.0 V, the sensor exhibits high sensitivity, reaching 33 and 42 %, respectively, for methanol, while demonstrating low sensitivities for ethanol and water molecules. Thus, the obtained sensitivities are larger compared to the sensitivities in the previous literature [48, 49]. This suggests that the sensor can selectively detect methanol as compared to ethanol and water molecules. Furthermore, the graphical representation of these sensitivities at various voltages is illustrated in Fig. 7.

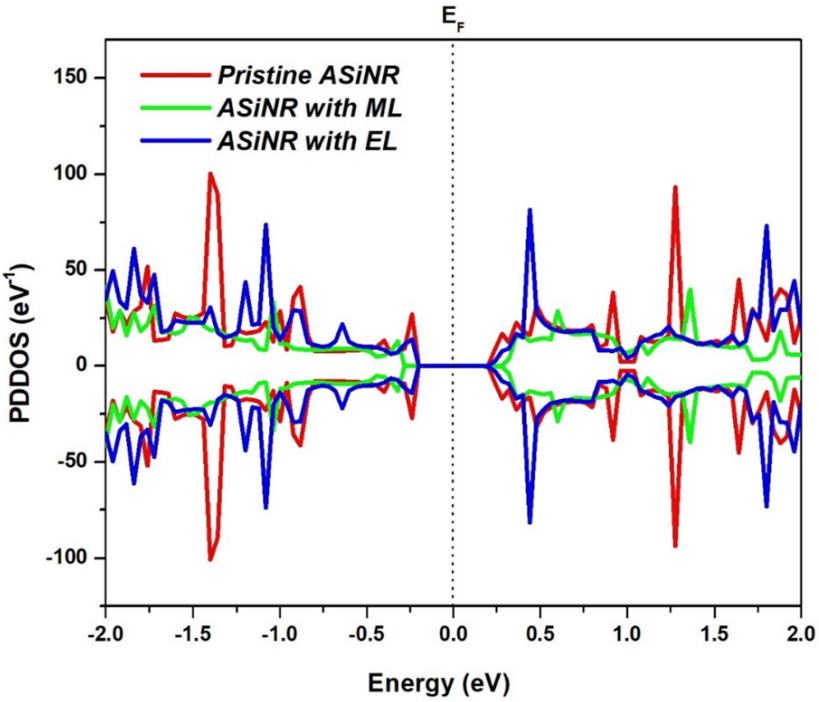

FIG. 6. Projected device density of states of ASiNR with and without adsorption of VOCs

TABLE 1. The calculated values of sensitivity (%) of the ASiNR sensor at bias voltages of (1.2, 1.4, 1.6, 1.8 and 2.0) V

Bias voltage	Target molecules		
	Methanol	Ethanol	Water
1.2 V	24	25	17
1.4 V	20	4.3	3.9
1.6 V	21	22	5.9
1.8 V	33	8.5	3.3
2.0 V	42	9.7	12.6

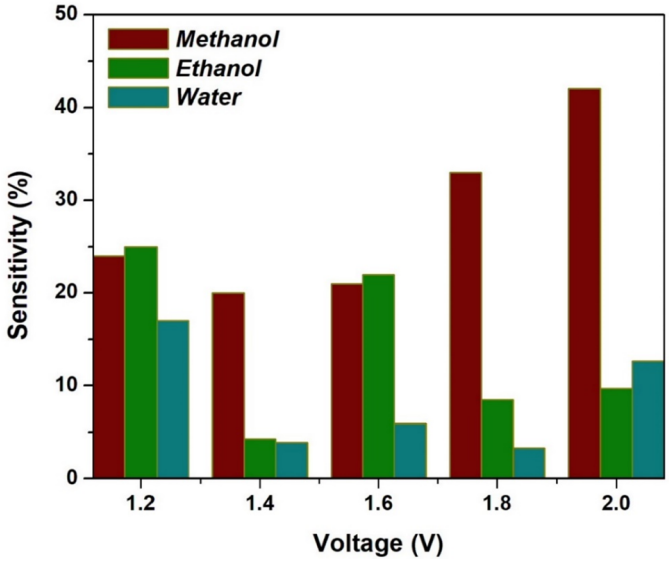

FIG. 7. Sensitivity of ASiNR sensor at different bias voltages

TABLE 2. Review of the proposed ASiNR sensor with other state of art sensors

2D Sensing Materials	**Analytes**	**Adsorption Energy (eV)**	**Sensor's Performance**	**References**
Graphene-like BC_6N	Acetone, Ethanol, Methanol, Formaldehyde, Toluene	-0.381, -0.378, -0.316, -0.228, -0.910	6.1 %, 14.7 %, 9.5 %, 14.7 %, 14.7 %	[9]
Defected-BC_6N	Acetone, Ethanol, Methanol, Formaldehyde, Toluene	-0.527, -0.754, -0.750, -0.647, -1.00	1.7 %, 61.0 %, 1.8 %, 15.4 %, 8.8 % (sensitivities) 740 s, 4.9 s, 4.2 s, 77 ms, 6800 s (recovery time)	[9]
Pristine-ASiNR	CH_4, CO_2, CO	-0.32, -0.59, -1.69	Not Given	[44]
Defective-ASiNR	CH_4, CO_2, CO	-0.45, -0.70, -1.94	Not Given	[44]
Silicene	Acetone, Toluene	Not Given	Not Given	[45]
Defected-Silicene	Isopropanol	Not Given	Not Given	[46]
C_3N Monolayer	Methanol, Ethanol, Acetone, Isopropanol, Isobutanol	-0.2408, -0.2203, 0.2531, -0.1225, -0.4359	26.96 %, 8.7 %, 71 % 59.5 %, 24.15 % (sensitivities)	[48]
Pristine Phosphorene	Acetone, Methanol, Ethanol, Toluene, CO_2, H_2O	-0.74, -0.67, -0.73, -1.16, -0.44, -0.54	1.27 %, 0.82 %, NR, NR (sensitivities) 2.67 s, 0.18 s, 1.81 s, $3.03 \cdot 10^7$ s, $2.45 \cdot 10^{-5}$ s, 0.001 s (recovery time)	[49]
Pd-decorated Phosphorene	Acetone, Methanol, Ethanol, Toluene, CO_2, H_2O	-1.14, -0.84, -1.06, -1.53, -0.45, -0.79	15.1 %, 14.3 %, NR, NR (sensitivities) $1.39 \cdot 10^7$ s, 127.94 s, $4.95 \cdot 10^{15}$ s, $4.95 \cdot 10^{13}$ s, $2.45 \cdot 10^{-5}$ s, 18.5 s (recovery time)	[49]
Al-doped GeS	Methanol, Ethanol	-0.379, -0.450	Not Given	[50]
Graphyne Nanosheet	Methanol, Ethanol	-0.167 to -0.532	Not Given	[52]
$MoSe_2$	Methanol, Ethanol	-0.375 to -0.732	Not Given	[53]
Pristine-ASiNR	NH_3	-0.49	Not Given	[67]
Silicene	Formaldehyde	-0.076	Not Given	[69]
ASiNR	**Methanol, Ethanol, H_2O**	-1.56, -1.62, -1.43	42 %, 9.7 %, 12.6 % (sensitivities) $2.4 \cdot 10^{14}$ s, $2.5 \cdot 10^{15}$ s, $1.5 \cdot 10^{12}$ s (recovery time)	**This Work**

3.1.6. Recovery time (τ). Another important parameter for a sensor is its reusability, which is related to the recovery time (τ) and relies on the adsorption energy (E_{ad}). In accordance with the conventional transition state theory, the recovery time τ can be described as [9, 68]:

$$\tau = \nu_0^{-1} \exp\left(-\frac{E_{ad}}{K_B T}\right), \tag{4}$$

where ν_0 is the attempt frequency, K_B is the Boltzmann constant and T is the operational temperature of sensor. In visible light ($\nu_0 = 10^{12}$ Hz) and at room temperature ($T = 298$ K), the stronger binding of ethanol ($E_{ad} = -1.62$ eV) compared to methanol ($E_{ad} = -1.56$ eV) and water ($E_{ad} = -1.43$ eV) implies that removing ethanol from the ASiNR sensor may be more challenging. By incorporating these parameters in Eq. (4), the obtained τ values are 2.4×10^{14} s for methanol, 2.5×10^{15} s for ethanol and 1.5×10^{12} s for water molecule. Consequently, it is basically impossible for the three molecules to desorb from the surface of ASiNR based device, it can be considered that the three molecules can stably exist in the ASiNR based device and are difficult to escape. The long desorption time shows that ASiNR based device has strong adsorption performance for the three molecules. Once the target molecules are captured by ASiNR, they will be hard to break free. Therefore, it can be used as an ideal adsorption material to remove the target molecules, showing great potential in the area of toxic gas scavenger.

The performance of the proposed sensor with that of other DFT based similar sensors mentioned in the literature is contrasted in Table 2. The table indicates that the interactions between VOCs and ASiNR are stronger than those with other 2D materials discussed in the literature such as graphene-like BC_6N [9], C_3N monolayer [48], pristine and Pd-decorated phosphorene [49], Al-doped GeS [50], graphyne nanosheet [52], $MOSe_2$ [53]. However, the proposed ASiNR sensor suffers an extremely longer recovery, which renders its application to be used as a reusable sensor.

4. Conclusion

In this study, we delved into the adsorption mechanism of human breath exhaled VOCs on the ASiNR based device. Our examination involves a meticulous exploration of the structural, electronic, and transport attributes of silicene. This study is perfoirmed by employing the advanced methodologies such as density functional theory and non-equilibrium Green's function (NEGF) formalism. The calculated adsorption energy (E_{ad}) follows the trend: ethanol $>$ methanol $>$ water. Additionally, we have identified substantial alterations in the transport properties resulting from the application of bias within the range of 0 to 2 V. Apart from that, we have also calculated the sensitivity (%), which confirms that methanol was highly sensitive as compared to the other molecules. Moreover, our analysis of the density of states demonstrates that ASiNR remains semiconducting both before and after adsorption, affirming the physisorption of the target molecules. Furthermore, although physisorption occurs, the ASiNR-based sensor exhibits a notably prolonged recovery time, suggesting challenges in desorbing molecules from the material's surface. This material positively influences the elimination of toxic gas molecules, highlighting ASiNR's significant potential in both detecting and removing toxic gases, making it suitable for disposable sensors and scavengers.

References

[1] Sun X., Shao K., Wang T. Detection of volatile organic compounds (VOCs) from exhaled breath as noninvasive methods for cancer diagnosis. *Analytical and Bioanalytical Chemistry*, 2016, **408**, P. 2759–2780.

[2] Mehdi Aghaei S., Aasi A., Panchapakesan B. Experimental and theoretical advances in MXene-based gas sensors. *ACS Omega*, 2021, **6** (4), P. 2450–2461.

[3] Aasi A., Mehdi Aghaei S., Panchapakesan B. Outstanding performance of transition-metal-decorated single-layer graphene-like BC6N nanosheets for disease biomarker detection in human breath. *ACS Omega*, 2021, **6** (7), P. 4696–4707.

[4] Das S., Pal M. Non-invasive monitoring of human health by exhaled breath analysis: A comprehensive review. *J. of The Electrochemical Society*, 2020, **167** (3), 037562.

[5] Hakim M., Broza Y.Y., Barash O., Peled N., Phillips M., Amann A., Haick H. Volatile Organic Compounds of Lung Cancer and Possible Biochemical Pathways. *Chem. Rev.*, 2012, **112**, P. 5949–5966.

[6] Kim J.S., Yoo H.W., Choi H.O., Jung H.T. Tunable volatile organic compounds sensor by using thiolated ligand conjugation on MoS_2. *Nano Letters*, 2014, **14** (10), P. 5941–5947.

[7] Chatterjee S., Castro M., Feller J.F. An e-nose made of carbon nanotube-based quantum resistive sensors for the detection of eighteen polar/nonpolar VOC biomarkers of lung cancer. *J. of Materials Chemistry B*, 2013, **1** (36), P. 4563–4575.

[8] Deng C., Zhang J., Yu X., Zhang W., Zhang X. Determination of acetone in human breath by gas chromatography–mass spectrometry and solid-phase microextraction with on-fiber derivatization. *J. of Chromatography B*, 2004, **810** (2), P. 269–275.

[9] Aghaei S.M., Aasi A., Farhangdoust S., Panchapakesan B. Graphene-like BC6N nanosheets are potential candidates for detection of volatile organic compounds (VOCs) in human breath: A DFT study. *Applied Surface Science*, 2021, **536**, 147756.

[10] Boots A.W., van Berkel J.J., Dallinga J.W., Smolinska A., Wouters E.F., van Schooten F.J. The versatile use of exhaled volatile organic compounds in human health and disease. *J. of breath research*, 2012, **6** (2), 027108.

[11] Atkinson R. Atmospheric chemistry of VOCs and NOx. *Atmospheric environment*, 2000, **34** (12–14), P. 2063–2101.

[12] Nagarajan V., Chandiramouli R.. First-Principles Investigation on Interaction of NH3 Gas on a Silicene Nanosheet Molecular Device. *IEEE Trans. Nanotechnology*, 2017, **16**, P. 445–452.

[13] Jariwala D., Sangwan V.K., Lauhon L.J., Marks T.J., Hersam M.C. Emerging Device Applications for Semiconducting Two-Dimensional Transition Metal Dichalcogenides. *ACS Nano*, 2014, **8**, P. 1102–1120.

[14] Nagarajan V., Chandiramouli R. CO and NO monitoring using pristine germanene nanosheets: DFT study. *J. Mol. Liq.*, 2017, **234**, P. 355–363.

[15] Nagarajan V., Chandiramouli R. Investigation of electronic properties and spin-orbit coupling effects on passivated stanene nanosheet: A first-principles study. *Superlattices Microstruct.*, 2017, **107**, P. 118–126.
[16] Ni Z., Liu Q., Tang K., Zheng J., Zhou J., Qin R., Gao Z., Yu D., Lu J. Tunable bandgap in silicene and germanene. *Nano Letters*, 2012, **12**, P. 113–118.
[17] Tao L., Cinquanta E., Chiappe D., Grazianetti C., Fanciulli M., Dubey M., Molle A., Akinwande D. Silicene field-effect transistors operating at room temperature. *Nature Nanotechnology*, 2015, **10**, P. 227–231.
[18] Tsai W.F., Huang C.-Y., Chang T.-R., Lin H., Jeng H.-T., Bansil A. Gated silicene as a tunable source of nearly 100 % spin-polarized electron. *Nat. Commun.*, 2013, **4** P. 1–6.
[19] Sadeghi H., Bailey S., Lambert C.J. Silicene-based DNA nucleobase sensing. *Applied Physics Letters*, 2014, **104**, 103104.
[20] Gao N., Zheng W.T., Jiang Q. Density functional theory calculations for two-dimensional silicene with halogen functionalization. *Physical Chemistry Chemical Physics*, 2012, **14**, P. 257–261.
[21] Lopez-Bezanilla A. Substitutional doping widens silicene gap. *J. Phys. Chem. C*, 2014, **118**, P. 18788–18792.
[22] Gao N., Li J.C., Jiang Q. Bandgap opening in silicene: Effect of substrates. *Chem. Phys. Lett.*, 2014, **592**, P. 222–226.
[23] Pan F., Wang Y., Jiang K., Ni Z., Ma J., Zheng J., Quhe R., Shi J., Yang J., Chen C., Lu J. Silicene nanomesh. *Scientific Reports*, 2015, **5**, 9075.
[24] Aghaei S.M., Monshi M.M., Torres I., Calizo I. Edge functionalization and doping effects on the stability, electronic and magnetic properties of silicene nanoribbons. *RSC advances*, 2016, **6**, P. 17046–17058.
[25] Aghaei S.M., Calizo I. Band gap tuning of armchair silicene nanoribbons using periodic hexagonal holes. *J. Appl. Phys.*, 2015, **118**, 104304.
[26] Kharadi M.A., Malik G.F., Shah K.A., Khanday F.A. Performance analysis of functionalized silicene nanoribbon-based photodetector. *Int. J. of Numerical Modelling: Electronic Networks, Devices and Fields*, 2021, **34**, e2809.
[27] Masson L., Prévot G. Epitaxial growth and structural properties of silicene and other 2D allotropes of Si. *Nanoscale Advances*, 2023, **5** (6), P. 1574–1599.
[28] Meng L., Wang Y., Zhang L., Du S., Wu R., Li L., Zhang Y., Li G., Zhou H., Hofer W.A., Gao M.J. Buckled silicene formation on Ir (111). *Nano Letters*, 2013, **13** (2), P. 685–690.
[29] Fleurence A., Friedlein R., Ozaki T., Kawai H., Wang Y., Takamura Y. Experimental evidence for epitaxial silicene on diboride thin films *Phys. Rev. Letters*, 2012, **108** (24), 24550.
[30] Aizawa T., Suehara S., Otani S. Silicene on zirconium carbide (111). *J. Phys. Chem. C*, 2014, **118** (40), 23049.
[31] Wang X.Q., Li H.D., Wang J.T. Induced ferromagnetism in one-side semi-hydrogenated silicene and germanene. *Phys. Chem. Chem. Phys.*, 2012, **14** (9), P. 3031–3036.
[32] Zheng F.B., Zhang C.W. The electronic and magnetic properties of functionalized silicene: a first-principles study. *Nanoscale Res. Letters*, 2012, **7**, P. 1–5.
[33] Liu C., Feng W., Yao Y. Quantum spin Hall effect in silicene and two-dimensional germanium. *Phys. Rev. Letters*, 2011, **107** (7), 076802.
[34] Xu C., Luo G., Liu Q., Zheng J., Zhang Z., Nagase S., Gao Z., Lu J. Giant magnetoresistance in silicene nanoribbons. *Nanoscale*, 2012, **4**, P. 3111–3317.
[35] Chen L., Feng B., Wu K. Observation of a possible superconducting gap in silicene on Ag (111), surface. *Appl. Phys. Letters*, 2013, **102** (8), 081602.
[36] Aufray B., Kara A., Vizzini S., Oughaddou H., Leandri C., Ealet B., Le Lay G. Graphene-like silicon nanoribbons on Ag (110): A possible formation of silicene. *Applied Physics Letters*, 2010, **96** (18), 183102.
[37] De Padova P., Quaresima C., Ottaviani C., Sheverdyaeva P.M., Moras P., Carbone C., Topwal D., Olivieri B., Kara A., Oughaddou H., Aufray B., Le Lay G. Evidence of graphene-like electronic signature in silicene nanoribbons. *Applied Physics Letters*, 2010, **96** (26), 261905.
[38] De Padova P., Kubo O., Olivieri B., Quaresima C., Nakayama T., Aono M., Le Lay G. Multilayer silicene nanoribbons. *Nano Letters*, 2012, **12** (11), P. 5500–5503.
[39] Tchalala M.R., Enriquez H., Mayne A.J., Kara A., Roth S., Silly M.G., Bendounan A., Sirotti F., Greber T., Aufray B., Dujardin G., Ali M.A., Oughaddou H. Formation of one-dimensional self-assembled silicon nanoribbons on Au (110),-(2$\times$ 1). *Applied Physics Letters*, 2013, **102** (8), 083107.
[40] Zha D., Chen C., Wu J. Electronic transport through a silicene-based zigzag and armchair junction. *Solid State Communications*, 2015, **219**, P. 21–24.
[41] Houssa M., van den Broek B., Scalise E., Pourtois G., Afanasev V.V., Stesmans A. An electric field tunable energy band gap at silicene/ (0001), ZnS interfaces. *Physical Chemistry Chemical Physics*, 2013, **15** (11), P. 3702–3705.
[42] Prasongkit J., Amorim R.G., Chakraborty S., Ahuja R., Scheicher R.H., Amornkitbamrung V. Highly Sensitive and Selective Gas Detection Based on Silicene. *J. Phys. Chem. C*, 2015, **119**, P. 16934–16940.
[43] Nagarajan V., Chandiramouli R. First-Principles Investigation on Interaction of NH3 Gas on a Silicene Nanosheet Molecular Device. *IEEE Trans. Nanotechnology*, 2017, **16**, P. 445–452.
[44] Walia G.K., Randhawa D.K.K. Gas-sensing properties of armchair silicene nanoribbons towards carbon-based gases with single-molecule resolution. *Struct. Chem.*, 2018, **29**, P. 1893–1902.
[45] Pham T.L., Ta T.L., Vo V.O., Dinh V.A. DFT Study on Adsorption of Acetone and Toluene on Silicene. *VNU J. of Science: Mathematics-Physics*, 2020, **36**, P. 95–102.
[46] Vo V.O., Pham T.L., Dinh V.A. Absorption of Isopropanol on Surface of Defect Silicene. *VNU J. of Science: Mathematics-Physics*, 2020, **36**, P. 92–99.
[47] Showket S., Shah K.A., Dar G.N. Pristine and Modified Silicene based Volatile Organic Compound Toxic Gas Sensor: A First Principles Study. *Physica Scripta*, 2023, **98**, 085937.
[48] Agrawal S., Kaushal G., Srivastava A. Electron transport in C3N monolayer: DFT analysis of volatile organic compound sensing. *Chemical Physics Letters*, 2021, **762**, 138121.
[49] Aasi A., Aghaei S.M., Bajgani S.E., Panchapakesan B. Computational Study on Sensing Properties of Pd?Decorated Phosphorene for Detecting Acetone, Ethanol, Methanol, and Toluene: A Density Functional Theory Investigation. *Advanced Theory and Simulations*, 2021, **4**, 2100256.
[50] Pu K., Dai X., Bu Y., Guo R., Tao W., Jia D., Song J., Zhao T., Feng L. Al-doped GeS nanosheet as a promising sensing material for O-contained volatile organic compounds detection. *Applied Surface Science*, 2020, **527**, 146797.
[51] Singsen S., Watwiangkham A., Ngamwongwan L., Fongkaew I., Jungthawan S., Suthirakun S. Defect Engineering of Green Phosphorene Nanosheets for Detecting Volatile Organic Compounds: A Computational Approach. *ACS Applied Nano Materials*, 2023, **6**, P. 1496–1506.
[52] Nagarajan V., Dharani S., Chandiramouli R. Density functional studies on the binding of methanol and ethanol molecules to graphyne nanosheet. *Comput. Theor. Chem.*, 2018, **1125**, P. 86–94.

[53] Nagarajan V., Chandiramouli R. $MoSe_2$ nanosheets for detection of methanol and ethanol vapors: a DFT study. *J. of Molecular Graphics and Modelling*, 2018, **81**, P. 97–105.
[54] Gani M., Shah K.A., Parah S.A. Realization of a sub-10 nm silicene magnetic tunnel junction and its application for magnetic random access memory and digital logic. *IEEE Transactions on Nanotechnology*, 2021, **20**, P. 466–473.
[55] URL: https://synopsys.com/silicon/quantumatk.html Synopsys Quantum ATK, P-2019.03, 2019.
[56] Zeng M., FengY., Liang G. Graphene-based spin caloritronics. *Nano Letters*, 2011 ,**11**, P. 1369–1373.
[57] Perdew J.P., Burke K., Ernzerhof M. Generalised gradient approximation made simple. *Phys. Rev. Lett.*, 1996, **77**, P. 3865–3868.
[58] Abadir G.B., Walus K., Pulfrey D.L. Basis-set choice for DFT/ NEGF simulations of carbon nanotubes. *J. Comp. Electron.*, 2009, **8**, P. 1–9
[59] Yamacli S. Comparison of the electronic transport properties of metallic graphene and silicene nanoribbons. *J. Nanopart. Res.*, 2014, **16**, 2576.
[60] Srivastava P., Jaiswal N.K., Tripathi G.K. Chlorine sensing properties of zigzag boron nitride nanoribbons. *Solid State Commun.*, 2014, **185**, P. 41–46.
[61] Wei X.L., Chen Y.P., Liu W.L., Zhong J.X. Enhanced gas sensor based on nitrogen-vacancy graphene nanoribbons. *Phys. Lett. A*, 2012, **376**, P. 559–562.
[62] Aghaei S.M., Monshi M.M., Calizo I. A theoretical study of gas adsorption on silicene nanoribbons and its application in a highly sensitive molecule sensor. *RSC*, 2016, **6**, P. 94417–94428.
[63] Ding Y., Ni J. Electronic structures of silicon nanoribbons. *Applied Physics Letters*, 2009, **95**, 083115.
[64] Davila M.E., Marele A., De Padova P., Montero I., Hennies F., Pietzsch A., Shariati M.N., Gomez Rodriguez J.M., Le Lay G. Comparative structural and electronic studies of hydrogen interaction with isolated versus ordered silicon nanoribbons grown on Ag (110). *Nanotechnology*, 2012, **23**, 385703.
[65] Osborn T.H., Farajian A.A., Pupyesheva O.V., Aga R.S., Voon L.L.Y. Ab initio simulations of silicene hydrogenation. *Chem. Phys. Lett.*, 2011, **511**, P. 101–105.
[66] Naqash A.N., Shah K.A., Sheikh J.A., Kumbhani B., Andrabi S.M. Transport properties of GaAs Co-doped H-passivated low-buckled and high-buckled zigzag silicene nanoribbon two probe devices. *Nanosystems: Physics, Chemistry, Mathematics*, 2023, **14** (4), P. 438–446.
[67] Walia G.K., Randhawa D.K.K. Electronic and transport properties of silicene-based ammonia nanosensors: an ab initio study. *Structural Chemistry*, 2018, **29**, P. 257–265.
[68] Walia G.K., Randhawa D.K.K. Gas sensing properties of armchair silicene nanoribbons towards carbon-based gases with single molecule resolution. *Structural Chemistry*, 2018, **29**, 1893.
[69] Wang X., Liu H., Tu S.T. Study of formaldehyde adsorption on silicene with point defects by DFT method. *RSC Advances*, 2015, **80**, P. 65255–65263.

Submitted 5 January 2024; revised 21 February 2024; accepted 7 April 2024

Information about the authors:

Shazia Showket – Department of Physics, University of Kashmir, Srinagar, J&K – 190006, India; ORCID 0009-0009-7438-2260; shaziashowket.phscholar@kashmiruniversity.net

Khurshed A. Shah – Postgraduate Department of Physics, Sri Pratap College, Cluster University Srinagar, J&K – 190001, India; ORCID 0000-0002-2694-4515; drkhursheda@gmail.com

Ghulam Nabi Dar – Department of Physics, University of Kashmir, Srinagar, J&K – 190006, India; ORCID 0000-0002-5066-0141; gndphy@kashmiruniversity.ac.in

Muzaffar Ali Andrabi – Department of Applied Sciences, Institute of Technology, University of Kashmir, Srinagar, J&K – 190006, India; ORCID 0009-0001-9584-3398; muzaffar2000@gmail.com

Conflict of interest: the authors declare no conflict of interest.